

Onset of strong coupling in site-controlled high C_{3v} -symmetric InGaAs QD-nanocavity on the (111)B-oriented GaAs membrane

Jiahui Huang^{1,†,*}, Wei Liu^{1,†,*}, Xiang Cheng¹, Alessio Miranda², Benjamin Dwir², Alok Rudra², Eli Kapon² and Chee Wei Wong^{1,*}

¹Mesoscopic Optics and Quantum Electronics Laboratory, University of California, Los Angeles, 420 Westwood Plaza, CA 90095, USA

²Institute of Physics, École Polytechnique Fédérale de Lausanne, Lausanne, VD 1015, Switzerland

*Correspondence: jiahuihuang@ucla.edu; weiliu01@lbl.gov; cheewei.wong@ucla.edu

†These authors contributed equally.

Precise positioning of single site-controlled InGaAs QD embedded in the (111)B-oriented GaAs PhC cavity, which enables high C_{3v} symmetries of QD with nanometer-scale accuracy offers great promise for on-chip photonic quantum information processing. However, achieving the strong coupling regime in this geometry is rarely reported due to the increase in cavity loss. Here, we reveal the onset of phonon-mediated coherent exciton-photon interaction on our tailored device. Our results present a Rabi-like oscillation of luminescence intensity between excitonic and photonic components correlated with their oscillatory energy splitting. Such Rabi-like oscillation is well reproduced by modeling the coherent exchange of the exciton-photon population. The modeling further reveals an oscillatory two-time covariance at QD-cavity resonance, which indicates the system operates at the onset of the strong coupling regime. Moreover, by using the cavity mode as a probe of the virtual state of QD induced by phonon scattering, it reveals an increase in phonon scattering rates near the QD-cavity resonance, which can result in the onset of the strong coupling regime disguised with a singlet spectral feature.

Introduction

Precise positioning of single inverted pyramidal quantum dots (QDs) in photonics crystal (PhC) cavities with nanometer-scale accuracy offer remarkable promise for on-chip integrated quantum photonic circuits [1], which holds unique advantages compared to the conventional self-assembled Stranski-Krastanov (SK) QDs [2]. Its deterministic QD nucleation and position control permit efficient light-matter interaction by placing a single QD at the antinode of cavity field distribution with nanometer accuracy [3]. Its high structural symmetry and growth mechanisms allow isotropic polarization, suppress the fine structure splitting, and avoid spurious cavity feedings due to the absence of parasitic QDs and wetting layers [3],[4]. The strongly coupled QD-cavity system has been proved as an emerging platform for quantum applications such as the on-demand generation of non-classical light through photon-induced tunneling and blockade via strong exciton-photon coupling [5]–[7] and spin-controlled quantum switch via strong QD spin-photon coupling [8]–[10]. In the weakly coupled case, the Purcell enhancement can improve the photon collection efficiency for entangled photon pairs through cavities [11]–[13]. In such coupled exciton-photon hybrid architecture, the decoherence, on one hand, fundamentally affects the quantum applications such as coherent control for unbreakable secure quantum communications

[14], quantum memory enabled single-photon switch [15],[16], coherent emitter-emitter coupling [17], and quantum network protocol based on deterministic cluster state generation [18],[19]. On the other hand, pure [20]–[23] and phonon-induced dephasing [24]–[29] also play important roles in the QD-cavity interacting dynamics, Jaynes-Cummings nonlinearities, and intermediate coupling regimes. However, to our knowledge, achieving the strong coupling regime and the impact of dephasing in strong exciton-photon interaction were mostly studied based on SK QDs [30]–[38], and it is rarely reported in site-controlled inverted pyramidal InGaAs QD-cavity. This is because (1) there is a trade-off between low-quality QD excitonic lines at increased Indium content and increased cavity Q -factor at longer wavelength [39]; (2) (111)B-oriented GaAs substrate and membrane, which is essential for etching high symmetric inverted pyramid for C_{3v} -symmetric QD epitaxy [3],[40], is subjected to an increased cavity loss compared to the (100)-oriented membrane. In this study, with increased Indium content and tailored pyramid size, the emission energy of our single site-controlled inverted pyramidal InGaAs/GaAs QD is pushed to ~ 1.24 eV with sub-100 μeV excitonic linewidth. At such photon energy, the reduced absorption losses from the Urbach tails of GaAs [41],[42] and smaller structural disorders from increased PhC holes radius lead to an increased Q -factor of our PhC cavities on (111)B-oriented membrane. Different from the previous studies [43]–[45] on site-controlled high symmetric QD-cavity suffered from low Q -factor (~ 3000) and thus operated in the weak coupling regime, based on our tailored device, we investigate the cavity quantum electrodynamics (cQED) operating at the onset of the strong coupling regime mediated by phonon induced dephasing via cryogenic micro-photoluminescence ($\mu\text{-PL}$) with multiple spectral-temporal-polarization resolutions and single photon second-order autocorrelation $g^{(2)}(\tau)$ interferometer. By tuning the QD-CM coupling via varying cryogenic temperatures, different from the typical weak coupling case, we demonstrate the spectral plateau when QD is brought in resonance with CM which flavors double Lorentzian fitting and reveals mutual linewidth narrowing of upper and lower energy components. We then present a cQED model which reveals the role of pure and phonon-induced dephasing in our system and confirms its operation at the onset of strong coupling. It can be further solidified by our experimental signatures of Rabi-like oscillation and quantum beating between the upper and lower energy components by varying the pump power which can be well reproduced by our modeling of the system's initial states. Such observation of the onset of strong coupling regime mediated by phonons in our device sheds light on the feasibility of using site-controlled inverted pyramidal InGaAs QD – (111)B-oriented PhC cavity system, previously usually operating in weak coupling regime, for nonlinear optics and coherent control for quantum information processing in the integrated quantum photonics.

Optical properties and recombination dynamics

We first characterize the $\mu\text{-PL}$ spectra of our site-controlled high symmetric QD - L7 photonic crystal cavity (PhC) cavity system. Figure 1(a) presents the $\mu\text{-PL}$ spectra of decoupled (red) and coupled QD-cavity (black) system measured at different sample temperatures, excited by a 900 nm pulsed diode laser with 40 μW average pump power. The QD excitonic linewidth is as narrow as 92 μeV at 20 K, meanwhile, the linewidth of fundamental cavity mode is about 111 μeV , which corresponds to a more than 10,000 Q factor of the L7 cavity much larger than previous reported values in [43]–[45]. We note that a low rate of excitonic dephasing and cavity dissipation, along with large coupling strength by accurately positioning the QD at the maximum of the cavity field is a prerequisite for strong exciton-photon coupling [31],[46]. The exciton emission can be resonantly coupled with cavity mode as temperature increases up to around 50 K.

The Purcell-enhanced coupled QD-CM PL intensity is about 8-fold larger than the decoupled excitonic PL intensity. In the inset of Figure 1(a), by performing Hanbury-Brown-and-Twiss (HBT) measurements with a 532 nm continuous wave laser, we verify the single photon emission characteristic with the degree of second-order coherence $g^{(2)}(\tau=0) \approx 0.42 < 0.5$ at QD-CM resonance, which supports that the coupled QD-CM is at the single-exciton and single-photon level. The non-zero $g^{(2)}(\tau=0)$ is likely due to the instrumental response of our HBT setup and above-bandgap pumping. Figure 1(b) examines the polarization features of the cavity mode and excitonic emission with a detuning of ~ 3.8 meV. Its inset illustrates the scanning electron microscope (SEM) image of the QD-cavity structure, where the dot-triangle sign labels the position of the inverted pyramidal QD. The luminescence through the cavity mode reveals a predominant vertical polarization resulting from the Purcell-enhanced TE mode (vertical polarization), in contrast to the suppression of TM mode emission. On the other hand, the QD excitonic emission exhibits anti-polarization (negative degree of linear polarization) with respect to that of the cavity mode. Such anti-polarization at large positive detuning can be resulted from either an off-resonant phonon-assisted cavity feeding effect, causing a redistribution of photon emission from the excitonic decay channel to TE mode [44], or from the certain continuum local density of states (LDOS) of the L7 cavity on (111)B-oriented membrane [3].

We further perform the time-resolved μ -PL (TRPL) with sub-bandgap 900 nm pulsed excitation at 20 MHz repetition rate with lower average power at 10 μ W to characterize the QD-cavity interaction dynamics at low injection. Figure 1(c) manifests a shortening of decay time from 2.5 ns of the decoupled QD excitonic decay to 1.2 ns of the resonantly coupled QD-CM PL, which indicates Purcell enhancement. The instrument response is about 0.5 ns, as verified by probing the laser pulse. In particular, the PL decay of the resonantly coupled QD-CM system reveals a slower decay at an early delay, which is likely linked to the coupled QD-CM dynamics [47]. As a comparison, the decay of decoupled excitonic PL is monoexponential and starts at an early delay, which confirms the absence of saturation of the QD in the low injection region. Figure 1(d) further presents the coupled QD-CM PL decay (linear scale of the Y axis) as a function of pump power from 5 μ W to 40 μ W. Up to 20 μ W, the QD-CM coupling-induced plateau at early time delay extends up to 2 ns with increasing power. Such QD-CM coupling-induced PL plateau at early delay suggests the efficient QD exciton and photon interaction in the cavity before decaying. As the power > 20 μ W, a secondary raising of PL intensity appears around 2 ns, which results from the finite p-state occupation of QD by carrier feeding [45].

Phonon dynamics and dephasing toward strong exciton-photon coupling regime

We subsequently characterize the μ -PL spectra of fine-tuning QD-cavity coupling near resonance by varying the sample's temperature as shown in Figure 2(a), with a much lower injection of 3 μ W to suppress free-carrier-induced charge fluctuation. Importantly, although the anti-crossing of QD-CM dispersion is not resolved, the coupled QD-cavity spectra exhibit a plateau that can be well fit by double-Lorentzian within a zero-detuning range of 47 K-48.05 K, which suggests the feature of approaching the strong-coupling regime [31]. As temperature increases, the upper energy component of the fitting results in a variation from an exciton-like dispersion to a cavity-mode-like one, and vice versa for the lower energy component. We further compare the fitting of spectra by single and double Lorentzian near zero-detuning, the latter of which reproduce more accurately (larger R-square values) the flattening PL peak induced by QD-cavity interaction at zero detuning as shown in Figure S1 in the Supplementary. It is worth noting that the typical doublet splitting in the strong

coupling regime can be concealed by pure dephasing, phonon scattering, and incoherent pumping, and thus disguise as a plateau or even a single peak in our QD-cavity system [20]. Figure 2(b) shows the extracted PL energies of the upper (red dot) and lower (blue dot) energy components as a function of temperature. Meanwhile, the hollow dot represents the energy of coupled QD-CM spectrum by the single Lorentzian fit. Accordingly, as shown in Figure 2(c), the intensity ratio of the upper and lower energy components to their summation appears averaging behavior near resonance as a feature of polariton [31]. Moreover, the cavity and exciton linewidth from the double-Lorentzian fitting, comparable at far-off resonance, exhibit a mutual narrowing near resonance from $\approx 90 \mu\text{eV}$ to $\approx 50 \mu\text{eV}$, which indicates suppression of dissipation of both upper and lower energy components as in Figure 2(d), which is in contrast to the typical linewidth averaging in the strongly coupled system with generally larger cavity loss than the excitonic pure dephasing rate [31],[48].

To study the impact of the dephasing mechanism (including fluctuating environmental charges and phonon scattering) in our QD-cavity system, we perform the cQED modeling with Quantum Optics Toolbox [49] to simulate the coupled QD-cavity PL spectrum as a function of detuning. In brief, the density matrix $\hat{\rho}$ of dephasing mediated QD-cavity interaction is described by the Lindblad master equation $\frac{d\hat{\rho}}{dt} = -\frac{i}{\hbar}[\hat{H}, \hat{\rho}] + \mathcal{L}(\hat{\rho})$, where $\hat{H} = \hbar\omega_c \hat{a}^\dagger \hat{a} + \frac{\hbar\omega_X}{2} \hat{\sigma}_z + \hbar g(\hat{a}^\dagger \hat{\sigma}_- + \hat{\sigma}_+ \hat{a})$ is the Jaynes-Cumming (JC) Hamiltonian with ω_c , ω_X , \hat{a} , and g denoted as the frequency of the cavity mode, transition frequency of the QD exciton, annihilation operator of the cavity photon, and QD-cavity coupling strength, respectively. $\hat{\sigma}_{+/-z}$ are the pseudospin operator of the two-level QD excitons. The environmental dephasing is incorporated in the Liouvillian superoperator $\mathcal{L}(\hat{\rho}) = \frac{\kappa_c}{2} \mathcal{L}_{\hat{a}}(\hat{\rho}) + \frac{\gamma_X}{2} \mathcal{L}_{\hat{\sigma}_-}(\hat{\rho}) + \frac{P_X}{2} \mathcal{L}_{\hat{\sigma}_+}(\hat{\rho}) + \frac{\gamma_{deph}}{2} (\hat{\sigma}_z \hat{\rho} \hat{\sigma}_z - \hat{\rho}) + \frac{P_{ph}}{2} \mathcal{L}_{\hat{\sigma}_- \hat{a}^\dagger}(\hat{\rho})$, where κ_c , γ_X , P_X , γ_{deph} , and P_{ph} are the cavity loss rate, exciton decay rate, QD incoherent pumping rate, exciton pure dephasing rate, and phonon-mediated-coupling rate from the QD to the cavity, respectively [50]. The superoperator $\mathcal{L}_{\hat{X}}$ with arbitrary operator \hat{X} in the subscript operating has the form $\mathcal{L}_{\hat{X}}(\hat{\rho}) = 2\hat{X}\hat{\rho}\hat{X}^\dagger - \hat{X}^\dagger\hat{X}\hat{\rho} - \hat{\rho}\hat{X}^\dagger\hat{X}$. The experimental PL spectrum can be modeled through a steady-state power spectrum of the QD-CM system, which relates to the Fourier transform of the two-time covariance function of the excitonic operator and photon operator to be the $S(\omega) = \int_{-\infty}^{\infty} \lim_{t \rightarrow \infty} \langle A(t+\tau)B(t) \rangle e^{-i\omega\tau} d\tau$ with $A, B = \hat{\sigma}_+, \hat{\sigma}_-, \hat{a}^\dagger, \hat{a}$. Note that only single QD is incorporated in the cavity with all surrounding QDs etched away, the parasitic cavity pumping in typical SK ensemble QDs is absent in our system.

Figure 3 (a) shows the ω_c and ω_X extracted from the spectrum modeling. In Figure 3 (b), we first adjusted κ_c to $80 \mu\text{eV}$ deconvolved system response to reproduce spectral linewidth of the cavity at the large detuning and keep constants for all temperatures (detuning). Similarly, γ_{deph} is set to be $30 \mu\text{eV}$ to match the QD exciton linewidth at the lower temperatures. We derive a slight increase of exciton pure dephasing γ_{deph} at 49 K, which can be attributed to a small increase of charge fluctuating of the environmental charges at higher temperatures, consequently revealing a broadening of exciton linewidth. The phonon scattering rate P_{ph} is treated as a fitting parameter to reproduce the experimental spectrum shown in Figure 2 (a). The coupling strength is adjusted to be $g = 18 \mu\text{eV}$ and kept constant for all fittings. Note that such coupling strength set our system at the onset of the strong coupling regime ($g \approx \kappa_c/4$) which is consistent with our observation of spectral plateau in Figure 2 (a) and (b) rather than explicit mode splitting. The P_{ph} manifests a raising from $2 \mu\text{eV}$ when approaching the QD-CM resonance and shows a plateau with $7 \mu\text{eV}$ at temperatures corresponding to

near-zero detuning (47.35 K – 48.4 K) and subsequently falls when gradually decoupling between QD and cavity, which indicates enhanced phonon scattering rate around near-zero detuning. Here, cavity mode can be regarded as a sensitive probe of virtual states of QD induced by the emission or absorption of a phonon [50], which continuously spread about 200 μeV around ZPL of QD exciton [40]. Therefore, the elevated P_{ph} between 47.35 K and 48.4 K is result of convolution of the energy range of QD virtual states with the CM linewidth. At CM-QD decoupled region, P_{ph} also exhibits a slight asymmetry between lower (46.7 – 47 K) and higher (48.4 – 49 K) temperatures, which reveals the subtle difference in the rate of absorbing and emitting a phonon for cavity feeding, and indicates that the phonon bath is not fully populated up to 50 K.

To better illustrate the significant impact of P_{ph} on phonon-assisted-cavity feeding at different detuning (temperatures), we present the modeled spectrum with various P_{ph} at larger detuning (45.5 K) and near-zero detuning (47.6 K) in Figure 3(c) and 3(d), respectively. At 45.5 K, if without considering phonon-mediated coupling ($P_{ph} = 0$, dashed line in fig. 3(c)), the QD emission is stronger than the cavity mode, which contrasts with the experiment (dot in fig. 3(c)). With slightly increasing P_{ph} from 0 to 0.9 μeV , the PL intensity of QD decreases pronouncedly as a result of phonon-mediated transferring of QD excitations to the cavity decay channel, and finally $P_{ph} = 1.8 \mu\text{eV}$ well converges the fitting to the experimental spectra. Similarly, at 47.6 K, the fitting is converged with a larger $P_{ph} = 7 \mu\text{eV}$ to well match both sides of spectral tails, which is consistent with the phonon scattering feature of the solid-state emitter. Our modeling well captures the subtle impact of phonon scattering on the QD-CM coupling. We further evaluate the steady state two-time covariance function of cavity photons $\phi(\tau) = \langle \hat{a}^\dagger(t + \tau), \hat{a}(t) \rangle$ near zero detuning as shown in the inset of Figure 3(d). It clearly shows an oscillation in τ with an exponentially damped envelope. The field correlation exhibits multiple local minimums in τ equivalent to the Rabi frequency [51] and marks the coherent exchange between photon and exciton fields in our system even operating at the onset of the strong coupling regime. The dissipation and pumping due to environmental interactions manifest the exponential damping that decorrelates the exciton and photon fields. It's worth noting if neglecting P_{ph} but treating exciton pure dephasing rate γ_{deph} as a fitting parameter to converge the fit to the experiment, the γ_{deph} needs to be forced to increase as QD-CM is decoupling, which leads to an unphysical circumstance. The fitting to the experimental spectrum with $P_{ph} = 0$ is detailed in the Supplementary IV. These results highlight the important role of phonon-mediated-coupling in our system operating at the onset of strong coupling subject to environmental interactions. In addition, we repeat the modeling of the temperature tuning QD-cavity spectra measured with a higher pump power at 30 μW detailed in Supplementary Material Section V to demonstrate the robustness of our modeling.

Rabi oscillation and quantum beating of coupled spectral components

To gain further insight into the interaction in the resonantly coupled QD-CM system, we perform pump power-dependent PL measurements with sub-bandgap 900 nm pulse pumping with fixed pulse duration at 100 ps when QD-cavity detuning is small. Figure 4 (a) shows the PL spectrum at 5, 7, and 9 μW , which presents clear PL intensity variation between the upper and lower energy components. As shown in Figure 4(b), by varying pump power, the PL intensity of upper and lower energy components fit by double Lorentzian fitting manifests an out-of-phase oscillation up to 20 μW ,

which resembles the Rabi-like oscillation and quantum beating between them. The three points marked by the arrow correspond to pump power in Figure 4 (a). Such oscillation vanishes beyond 20 μW likely resulting from the increase of environmental charge fluctuation and incoherent excitation, which is consistent with the power-dependent TRPL results in Figure 1(d), where significant carrier feeding above 20 μW causes the decoherence of QD-cavity interaction. The energy separation between the lower and upper energy components by double Lorentzian fits also exhibits an oscillatory signature correlated with the intensity oscillation, shown as black spheres in Figure S5 in Supplementary Section VI. To explain the oscillation behavior, we model the QD-CM coupled PL spectrum by varying the initial occupation state of the system, which is correlated with the changing pulse area in the experiment. In brief, the initial state of the system can be set by the weighting factor x in the superposition of QD exciton and cavity photon operator $x\hat{\sigma}_z + (1 - x)\hat{a}$, where x denotes the initial occupation percentage of QD excitons which is complementary to the cavity photons. By varying x and calculating the cavity output spectra, our model well captures the variation of the measured PL spectrum at different pump power. The three representative modeled spectra fit the experiments at 5, 7, and 9 μW are shown as black solid lineshapes in Figure 4(a). In Figure 4(c), the initial occupation of QD excitons is plotted as red dots with the corresponding extracted QD-cavity energy splitting ΔE as black dots from the modeling. Importantly, we note that the lower occupation of QD excitons as an initial state of the system corresponds to a large splitting between the upper and lower components, and vice versa, which leads to an out-of-phase pump power dependent oscillation of the initial occupation of exciton and ΔE in Figure 4(c). Such behavior of PL intensity beating and splitting oscillation is consistent with the prior theoretical prediction [51] of the spectral shape evolution with the initial state as one exciton or one photon in a strongly coupled system. Note that complete photon domination ($x = 0$) of the system appears as pump power increases to around 4.5 μW in the first oscillation period but smears out in the following oscillation period. Such drops in the visibility at higher pump power are in line with the blurred PL intensity oscillation and thus the decoherence of QD-cavity interaction due to increased carrier feeding. It's worth noting that increasing QD-cavity detuning above 100 μeV reduces the contrast of the observed PL intensity and ΔE oscillation signature as shown in Figure S6 (b) and (c) in Supplementary VII, which suggests that the observed oscillation signature only remarkable at smaller detuning is correlated with coherent energy exchange in our system operating even at the onset of strong coupling mediated by phonons. In the temporal domain, it corresponds to the observed slow PL decay component or plateau at early time delay in Figure 1(c) which is only observable when QD exciton and CM are in resonance. It suggests a real-time oscillation of the energy between the QD exciton and the cavity photon, which is not experimentally resolved likely due to the relatively limited timing resolution of the setup and non-resonant pumping. The observed pump power-dependent Rabi-like oscillation indicates the feasibility of the initialization of our QD-CM system.

Conclusion

High symmetric patterned inverted pyramid on GaAs (111)B-oriented substrate for single site-controlled C_{3v} -symmetric InGaAs QD epitaxy and deterministic PhC cavity integration offers great promise for integrated quantum photonics. However, this geometry is subjected to increased cavity loss in contrast to the (100)-oriented membrane. In this study, we investigate the cQED in our tailored single site-controlled inverted pyramidal InGaAs QD-nanocavities system on the (111)B-oriented membrane operating at the onset of the strong coupling regime disguised with a singlet spectral

feature. Double Lorentzian fitting which is favored mathematically leads to the mutual linewidth narrowing of the upper and lower energy components near resonance. Further cQED modeling of the power spectra involving environmental dephasing reveals the pronounced phonon-mediated-coupling rate and an oscillatory two-time covariance function near zero QD-cavity detunings. It indicates that our phonon-mediated QD-cavity, even at the onset of strong coupling, supports the coherent exchange of exciton and photons. It is further substantiated in the pump pulse area-dependent PL measurement that we present the signatures of Rabi-like out-of-phase oscillation and quantum beating between emission intensity of the upper and lower energy components which is also correlated with an oscillatory feature of their energy splitting, occurring primarily at small QD-cavity detuning and lower pump power. The oscillation of energy splitting of upper and lower components can be well reproduced by modeling the initial occupation of excitons in the system. Our results demonstrate the feasibility of single site-controlled high symmetric InGaAs QD integrated into a (111)B-oriented PhC cavity towards the strong coupling regime and the necessitates to further optimize the fabrication process to suppress the cavity loss in this geometry. It enables and extends the applications of such systems to schemes for coherent control of the site-controlled exciton and photon states for quantum information processing in the integrated quantum photonic circuitry.

Supplementary material

The fabrication of site-controlled inverted pyramidal InGaAs QD – L7 cavity, μ PL measurement schematic, and additional experimental data analysis can be found in the accompanying supplementary material.

Reference

- [1] Juska, G., Dimastrodonato, V., Mereni, L. O., Gocalinska, A. & Pelucchi, E. Towards Quantum-Dot Arrays of Entangled Photon Emitters. *Nat. Photonics* **7**, 527–531 (2013).
- [2] Kiravittaya, S., Rastelli, A. & Schmidt, O. G. Advanced Quantum Dot Configurations. *Reports Prog. Phys.* **72**, 046502 (2009).
- [3] Čalić, M. Cavity Quantum Electrodynamics with Site-Controlled Pyramidal Quantum Dots in Photonic Crystal Cavities. *PhD thesis, EPFL* **5957**, (2013).
- [4] Winger, M., Volz, T., Tarel, G., Portolan, S., Badolato, A., Hennessy, K. J., Hu, E. L., Beveratos, A., Finley, J., Savona, V. & Imamoglu, A. Explanation of Photon Correlations in the Far-off-Resonance Optical Emission from a Quantum-Dot-Cavity System. *Phys. Rev. Lett.* **103**, (2009).
- [5] Faraon, A., Fushman, I., Englund, D., Stoltz, N., Petroff, P. & Vučković, J. Coherent Generation of Non-Classical Light on a Chip via Photon-Induced Tunnelling and Blockade. *Nat. Phys.* **4**, 859–863 (2008).
- [6] Faraon, A., Majumdar, A. & Vučković, J. Generation of Nonclassical States of Light via Photon Blockade in Optical Nanocavities. *Phys. Rev. A* **81**, 033838 (2010).
- [7] Majumdar, A., Bajcsy, M. & Vuckovic, J. Probing the Ladder of Dressed States and Nonclassical Light Generation in Quantum Dot-Cavity QED. *Phys. Rev. A - At. Mol. Opt. Phys.* **85**, 041801 (2011).
- [8] Sun, S., Kim, H., Solomon, G. S. & Waks, E. A Quantum Phase Switch between a Single Solid-State Spin and a Photon. *Nat. Nanotechnol.* **11**, 539–544 (2016).
- [9] Javadi, A., Ding, D., Appel, M. H., Mahmoodian, S., Löbl, M. C., Söllner, I., Schott, R., Papon, C., Pregiolato, T., Stobbe, S., Midolo, L., Schröder, T., Wieck, A. D., Ludwig, A., Warburton, R. J. & Lodahl, P. Spin-Photon Interface and Spin-Controlled Photon Switching in a Nanobeam Waveguide. *Nat. Nanotechnol.* **13**, 398–403 (2017).
- [10] Wells, L. M., Kalliakos, S., Villa, B., Ellis, D. J. P., Stevenson, R. M., Bennett, A. J., Farrer, I., Ritchie, D. A. & Shields, A. J. Photon Phase Shift at the Few-Photon Level and Optical Switching by a Quantum Dot in a Microcavity. *Phys. Rev. Appl.* **11**, 061001 (2019).
- [11] Dousse, A., Suffczyński, J., Beveratos, A., Krebs, O., Lemaître, A., Sagnes, I., Bloch, J., Voisin, P. & Senellart, P. Ultrabright Source of Entangled Photon Pairs. *Nat.* **2010 4667303** **466**, 217–220 (2010).
- [12] Versteegh, M. A. M., Reimer, M. E., Jöns, K. D., Dalacu, D., Poole, P. J., Gulinatti, A., Giudice, A. & Zwiller, V. Observation of Strongly Entangled Photon Pairs from a Nanowire Quantum Dot. *Nat. Commun.* **5**, 5298

(2014).

- [13] Huber, T., Predojević, A., Khoshnegar, M., Dalacu, D., Poole, P. J., Majedi, H. & Weihs, G. Polarization Entangled Photons from Quantum Dots Embedded in Nanowires. *Nano Lett.* **14**, 7107–7114 (2014).
- [14] Mabuchi, H. & Doherty, A. C. Cavity Quantum Electrodynamics: Coherence in Context. *Science (80-.)*. **298**, 1372–1377 (2002).
- [15] Sun, S., Kim, H., Luo, Z., Solomon, G. S. & Waks, E. A Single-Photon Switch and Transistor Enabled by a Solid-State Quantum Memory. *Science (80-.)*. **361**, 57–60 (2018).
- [16] Pscherer, A., Meierhofer, M., Wang, D., Kelkar, H., Martín-Cano, D., Utikal, T., Götzinger, S. & Sandoghdar, V. Single-Molecule Vacuum Rabi Splitting: Four-Wave Mixing and Optical Switching at the Single-Photon Level. *Phys. Rev. Lett.* **127**, (2021).
- [17] Rezus, Y. L. A., Walt, S. G., Lettow, R., Renn, A., Zumofen, G., Götzinger, S. & Sandoghdar, V. Single-Photon Spectroscopy of a Single Molecule. *Phys. Rev. Lett.* **108**, 093601 (2012).
- [18] Gimeno-Segovia, M., Rudolph, T. & Economou, S. E. Deterministic Generation of Large-Scale Entangled Photonic Cluster State from Interacting Solid State Emitters. *Phys. Rev. Lett.* **123**, 070501 (2019).
- [19] Schwartz, I., Cogan, D., Schmidgall, E. R., Don, Y., Gantz, L., Kenneth, O., Lindner, N. H. & Gershoni, D. Deterministic Generation of a Cluster State of Entangled Photons. *Science (80-.)*. **354**, 434–437 (2016).
- [20] Laucht, A., Hauke, N., Villas-Bôas, J. M., Hofbauer, F., Böhm, G., Kaniber, M. & Finley, J. J. Dephasing of Exciton Polaritons in Photoexcited InGaAs Quantum Dots in GaAs Nanocavities. *Phys. Rev. Lett.* **103**, 087405 (2009).
- [21] Gonzalez-Tudela, A., del Valle, E., Cancellieri, E., Tejedor, C., Sanvitto, D. & Laussy, F. P. Effect of Pure Dephasing on the Jaynes-Cummings Nonlinearities. *Opt. Express* **18**, 7002 (2010).
- [22] Auffèves, A., Gerace, D., Gérard, J.-M., Santos, M. F., Andreani, L. C. & Poizat, J.-P. Controlling the Dynamics of a Coupled Atom-Cavity System by Pure Dephasing. *Phys. Rev. B* **81**, 245419 (2010).
- [23] Vagov, A., Glässl, M., Croitoru, M. D., Axt, V. M. & Kuhn, T. Competition between Pure Dephasing and Photon Losses in the Dynamics of a Dot-Cavity System. *Phys. Rev. B* **90**, 075309 (2014).
- [24] Morreau, A. & Muljarov, E. A. Phonon-Induced Dephasing in Quantum-Dot-Cavity QED. *Phys. Rev. B* **100**, 115309 (2019).
- [25] Echeverri-Arteaga, S., Vinck-Posada, H. & Gómez, E. A. Explanation of the Quantum Phenomenon of Off-Resonant Cavity-Mode Emission. *Phys. Rev. A* **97**, 43815 (2018).
- [26] Echeverri-Arteaga, S., Vinck-Posada, H. & Gómez, E. A. The Strange Attraction Phenomenon in CQED: The Intermediate Quantum Coupling Regime. *Optik (Stuttg.)*. **183**, 389–394 (2019).
- [27] Calic, M., Gallo, P., Felici, M., Atlasov, K. A., Dwir, B., Rudra, A., Biasiol, G., Sorba, L., Tarel, G., Savona, V. & Kapon, E. Phonon-Mediated Coupling of InGaAs/GaAs Quantum-Dot Excitons to Photonic Crystal Cavities. *Phys. Rev. Lett.* **106**, 227402 (2011).
- [28] Ates, S., Ulrich, S. M., Ulhaq, A., Reitzenstein, S., Löffler, A., Höfling, S., Forchel, A. & Michler, P. Non-Resonant Dot-Cavity Coupling and Its Potential for Resonant Single-Quantum-Dot Spectroscopy. *Nat. Photonics* **3**, 724–728 (2009).
- [29] Hohenester, U., Laucht, A., Kaniber, M., Hauke, N., Neumann, A., Mohtashami, A., Seliger, M., Bichler, M. & Finley, J. J. Phonon-Assisted Transitions from Quantum Dot Excitons to Cavity Photons. *Phys. Rev. B* **80**, 201311 (2009).
- [30] Gao, J., Combric, S., Liang, B., Schmitteckert, P., Lehoucq, G., Xavier, S., Xu, X., Busch, K., Huffaker, D. L., De Rossi, A. & Wong, C. W. Strongly Coupled Slow-Light Polaritons in One-Dimensional Disordered Localized States. *Sci. Rep.* **3**, 1–6 (2013).
- [31] Reithmaier, J. P., Sek, G., Löffler, A., Hofmann, C., Kuhn, S., Reitzenstein, S., Keldysh, L. V., Kulakovskii, V. D., Reinecke, T. L. & Forchel, A. Strong Coupling in a Single Quantum Dot-Semiconductor Microcavity System. *Nature* **432**, 197–200 (2004).
- [32] Hennessy, K., Badolato, A., Winger, M., Gerace, D., Atatüre, M., Gulde, S., Fält, S., Hu, E. L. & Imamoglu, A. Quantum Nature of a Strongly Coupled Single Quantum Dot-Cavity System. *Nature* **445**, 896–899 (2007).
- [33] Yoshle, T., Scherer, A., Hendrickson, J., Khitrova, G., Gibbs, H. M., Rupper, G., Ell, C., Shchekin, O. B. & Deppe, D. G. Vacuum Rabi Splitting with a Single Quantum Dot in a Photonic Crystal Nanocavity. *Nature* **432**, 200–203 (2004).
- [34] Kasprzak, J., Reitzenstein, S., Muljarov, E. A., Kistner, C., Schneider, C., Strauss, M., Höfling, S., Forchel, A. & Langbein, W. Up on the Jaynes-Cummings Ladder of a Quantum-Dot/Microcavity System. *Nat. Mater.* **9**, 304–308 (2010).

- [35] Reithmaier, J. P. Strong Exciton–Photon Coupling in Semiconductor Quantum Dot Systems. *Semicond. Sci. Technol.* **23**, 123001 (2008).
- [36] Osada, A., Ota, Y., Katsumi, R., Kakuda, M., Iwamoto, S. & Arakawa, Y. Strongly Coupled Single-Quantum-Dot–Cavity System Integrated on a CMOS-Processed Silicon Photonic Chip. *Phys. Rev. Appl.* **11**, 024071 (2019).
- [37] Najer, D., Söllner, I., Sekatski, P., Dolique, V., Löbl, M. C., Riedel, D., Schott, R., Starosielec, S., Valentin, S. R., Wieck, A. D., Sangouard, N., Ludwig, A. & Warburton, R. J. A Gated Quantum Dot Strongly Coupled to an Optical Microcavity. *Nature* **575**, 622–627 (2019).
- [38] Lodahl, P., Mahmoodian, S. & Stobbe, S. Interfacing Single Photons and Single Quantum Dots with Photonic Nanostructures. *Rev. Mod. Phys.* **87**, 347–400 (2013).
- [39] Delgoffe, A. M. Functional Elements for Quantum-Dot-Based Integrated Quantum Photonics. (2020). doi:10.5075/EPFL-THESIS-7533
- [40] Jarlov, C. Cavity Quantum Electrodynamics with Systems of Site-Controlled Quantum Dots and Photonic Crystal Cavities. *PhD thesis, EPFL* **7039**, (2016).
- [41] Urbach, F. The Long-Wavelength Edge of Photographic Sensitivity and of the Electronic Absorption of Solids. *Phys. Rev.* **92**, 1324–1324 (1953).
- [42] John, S., Soukoulis, C., Cohen, M. H. & Economou, E. N. Theory of Electron Band Tails and the Urbach Optical-Absorption Edge. *Phys. Rev. Lett.* **57**, 1777–1780 (1986).
- [43] Jarlov, C., Wodey, Lyasota, A., Calic, M., Gallo, P., Dwir, B., Rudra, A. & Kapon, E. Effect of Pure Dephasing and Phonon Scattering on the Coupling of Semiconductor Quantum Dots to Optical Cavities. *Phys. Rev. Lett.* **117**, 076801 (2016).
- [44] Calic, M., Gallo, P., Felici, M., Atlasov, K. A., Dwir, B., Rudra, A., Biasiol, G., Sorba, L., Tarel, G., Savona, V. & Kapon, E. Phonon-Mediated Coupling of InGaAs/GaAs Quantum-Dot Excitons to Photonic Crystal Cavities. *Phys. Rev. Lett.* **106**, 227402 (2011).
- [45] Jarlov, C., Lyasota, A., Ferrier, L., Gallo, P., Dwir, B., Rudra, A. & Kapon, E. Exciton Dynamics in a Site-Controlled Quantum Dot Coupled to a Photonic Crystal Cavity. *Appl. Phys. Lett.* **107**, 191101 (2015).
- [46] Khitrova, G., Gibbs, H. M., Kira, M., Koch, S. W. & Scherer, A. Vacuum Rabi Splitting in Semiconductors. *Nat. Phys.* **2**, 81–90 (2006).
- [47] Schaibley, J. R., Burgers, A. P., McCracken, G. A., Steel, D. G., Bracker, A. S., Gammon, D. & Sham, L. J. Direct Detection of Time-Resolved Rabi Oscillations in a Single Quantum Dot via Resonance Fluorescence. *Phys. Rev. B* **87**, 115311 (2013).
- [48] Press, D., Götzinger, S., Reitzenstein, S., Hofmann, C., Löffler, A., Kamp, M., Forchel, A. & Yamamoto, Y. Photon Antibunching from a Single Quantum-Dot-Microcavity System in the Strong Coupling Regime. *Phys. Rev. Lett.* **98**, 117402 (2007).
- [49] Tan, S. M. Computational Toolbox for Quantum and Atomic Optics. *J. Opt. B Quantum Semiclassical Opt.* **1**, 424–432 (1999).
- [50] Majumdar, A., Kim, E. D., Gong, Y., Bajcsy, M. & Vučković, J. Phonon Mediated Off-Resonant Quantum Dot–Cavity Coupling under Resonant Excitation of the Quantum Dot. *Phys. Rev. B* **84**, 085309 (2011).
- [51] Laussy, F. P., del Valle, E. & Tejedor, C. Luminescence Spectra of Quantum Dots in Microcavities. I. Bosons. *Phys. Rev. B* **79**, 235325 (2009).

ACKNOWLEDGEMENT

The authors thank helpful discussions with Murat Can Sarihan, Abhinav Kumar Vinod, James F. McMillan, Yujin Cho, Kai-Chi Chang, Jin Ho Kang, Justin Caram, and Baolai Liang from UCLA and technical help from Alexey Lyasota and Bruno Rigal from EPFL in the sample fabrication. The authors also acknowledge exchange discussions with Sophia Economou and Bikun Li. J.H., W.L., and C.W.W. acknowledge support from the Army Research Office MURI (W91INF-21-2-0214) and National Science Foundation (2137984, 1936375, and 1919355). W.L. also acknowledges support from the Swiss National Science Foundation under project 187963. W.L. and J.H. led the project and performed the measurements with data analysis and cQED modeling. X.C supported the cQED modeling. B.D. and E.K. designed the samples. A.M., B. D., and A. R. grew the samples and performed the photonic crystal microcavity fabrication. C.W.W. and E.K. aided in the project. W.L., J.H., and C.W.W. wrote the manuscript, with contributions from all authors.

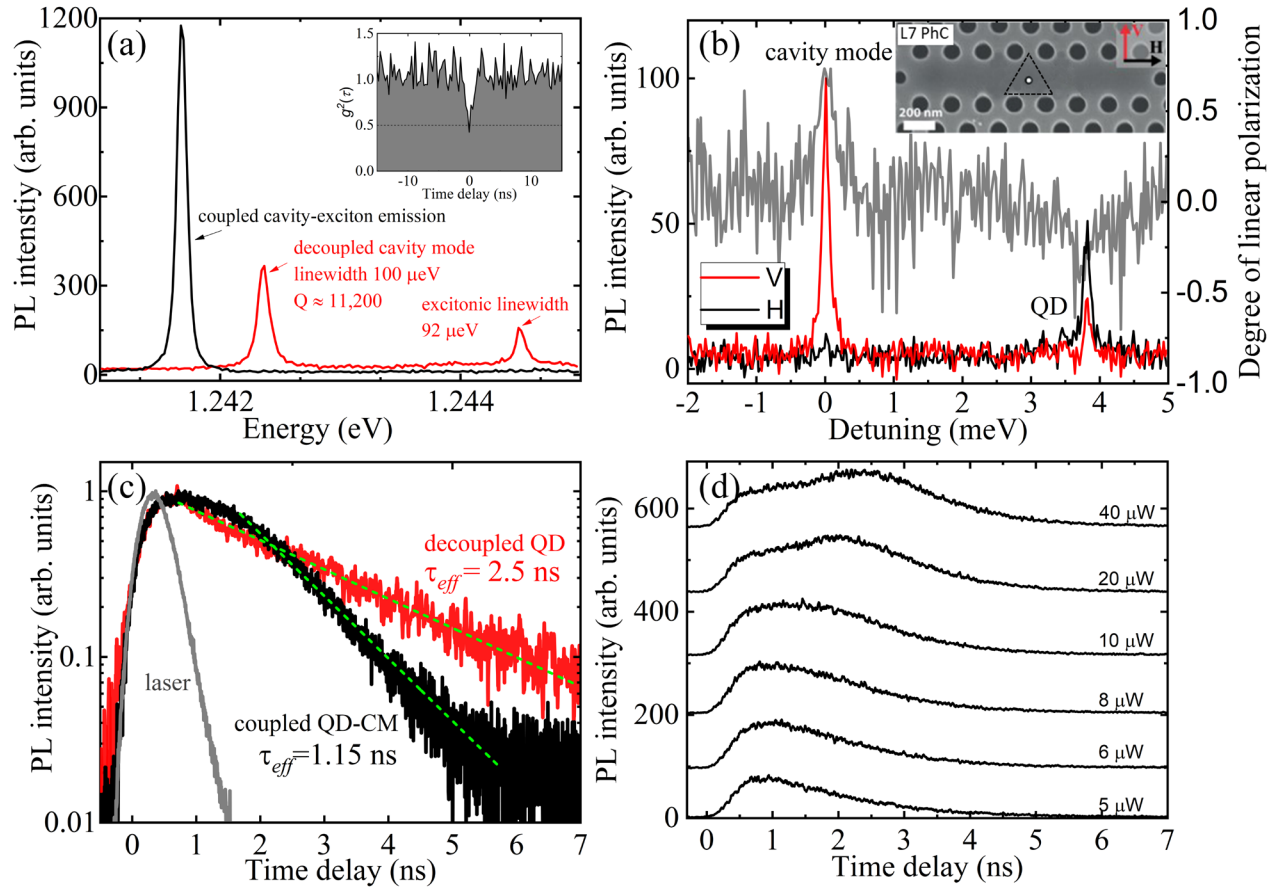


Figure 1 Optical properties and recombination dynamics (a) μ -PL spectra of decoupled (red) and coupled QD-cavity (black) system. Inset: Second-order correlation function of the coupled QD-cavity emission. (b) μ -PL of TE and TM cavity mode and QD single excitonic line, with vertical (red) and horizontal (black) polarization. The grey line indicates the degree of linear polarization $P = (I_V - I_H)/(I_V + I_H)$. Inset: SEM image of single site-controlled QD - L7 photonic crystal cavity, where the position of pyramidal QD, as dot-triangle labeling, matches the antinode of the cavity field distribution. (c) PL decay of decoupled excitonic emission (red) and coupled QD-CM (black), corresponding to 2.46 ns and 1.15 ns decay time, extracted by single exponential decay, respectively. The grey decay curve records the laser decay, which suggests an about 500 ps instrument response. (d) PL decay of the resonantly coupled QD-CM as a function of pump power.

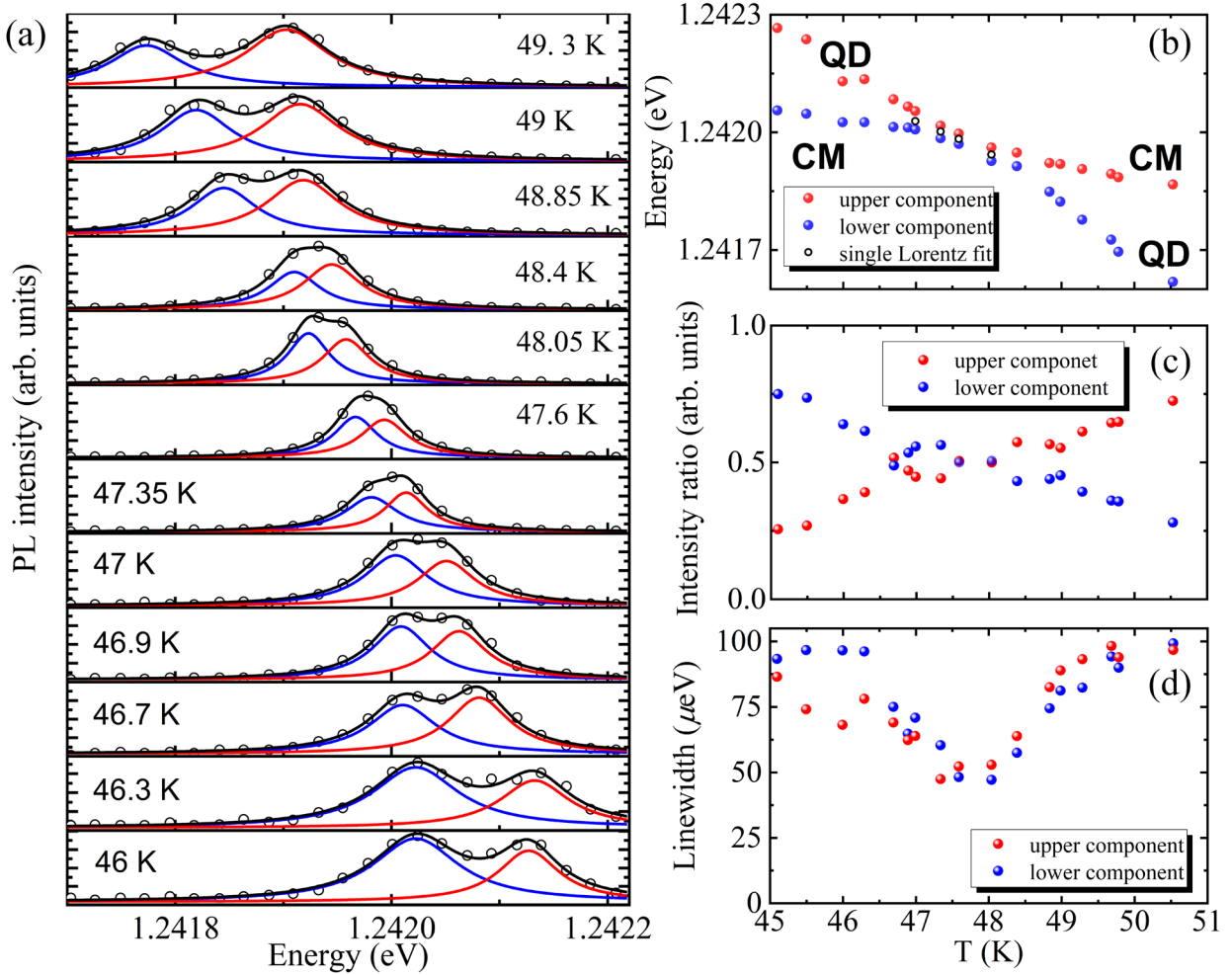


Figure 2 Temperature tuning of QD-cavity coupling (a) PL spectra (circle) of the coupled QD and CM around resonance fine detuned by varying temperature. The blue and red curves represent the double Lorentzian fitting, and the black curve is their cumulative fit. (b) Dependences of PL peak energies of coupled QD-cavity system over a wide temperature range. The single Lorentzian fit corresponds to black hollow circles as shown in Figure S1 in the supplementary. The exciton and CM dispersion resemble the polariton-like feature with upper (red dot) and lower (blue dot) energy components extracted by double Lorentzian fitting, indicating an approaching strong-coupling regime of the system. (c) the corresponding detuning dependent PL intensity ratio between the upper and lower energy components to their summation, which reveals averaging at near resonance. (d) The corresponding detuning-dependent linewidth of the upper and lower energy components presents mutual narrowing.

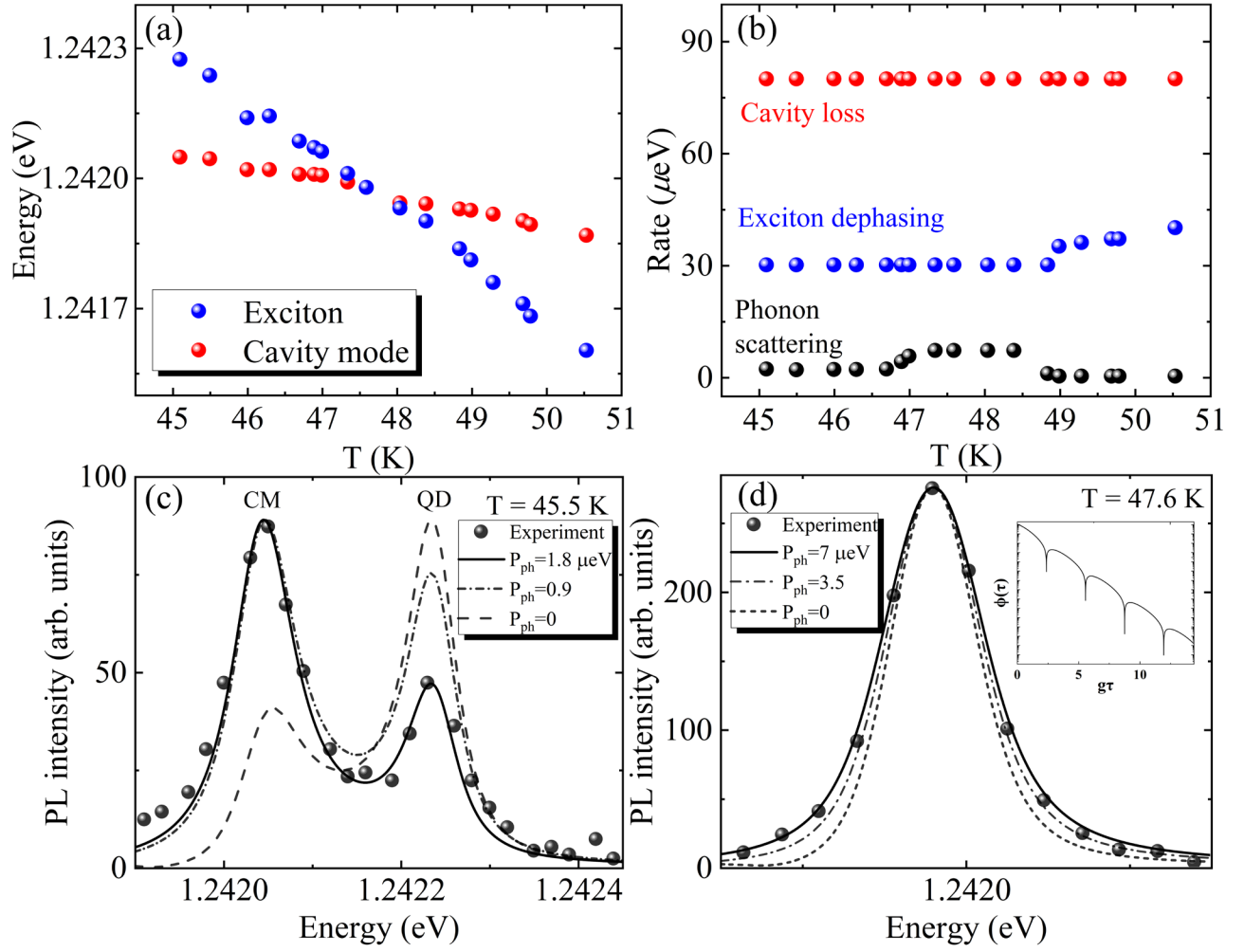


Figure 3 cQED modeling of phonon mediated QD-cavity coupling (a) Fitting of energy of exciton (blue) and cavity mode (red) as a function of temperature in Figure 2(a) by the cQED modeling. (b) Cavity loss (red), exciton dephasing (blue), and phonon scattering (black) rate as a function of temperature in the QD-cavity system extracted from the modeling in (a). (c) PL spectra (dot) of the decoupled QD-cavity system at 45.5 K. The dash, dot-dash, and solid lines are the fitting corresponding to the phonon-mediated QD-cavity coupling rate $P_{ph}=0, 0.9$, and $1.8 \mu\text{eV}$, respectively. (d) PL spectra (dot) of the resonantly coupled QD-cavity system at 47.6 K. The dash, dot-dash, and solid lines are the fitting corresponding to the phonon-mediated QD-cavity coupling rate $P_{ph}=0, 3.5$, and $7 \mu\text{eV}$, respectively. Inset: Time evolution of the corresponding two-time covariance function.

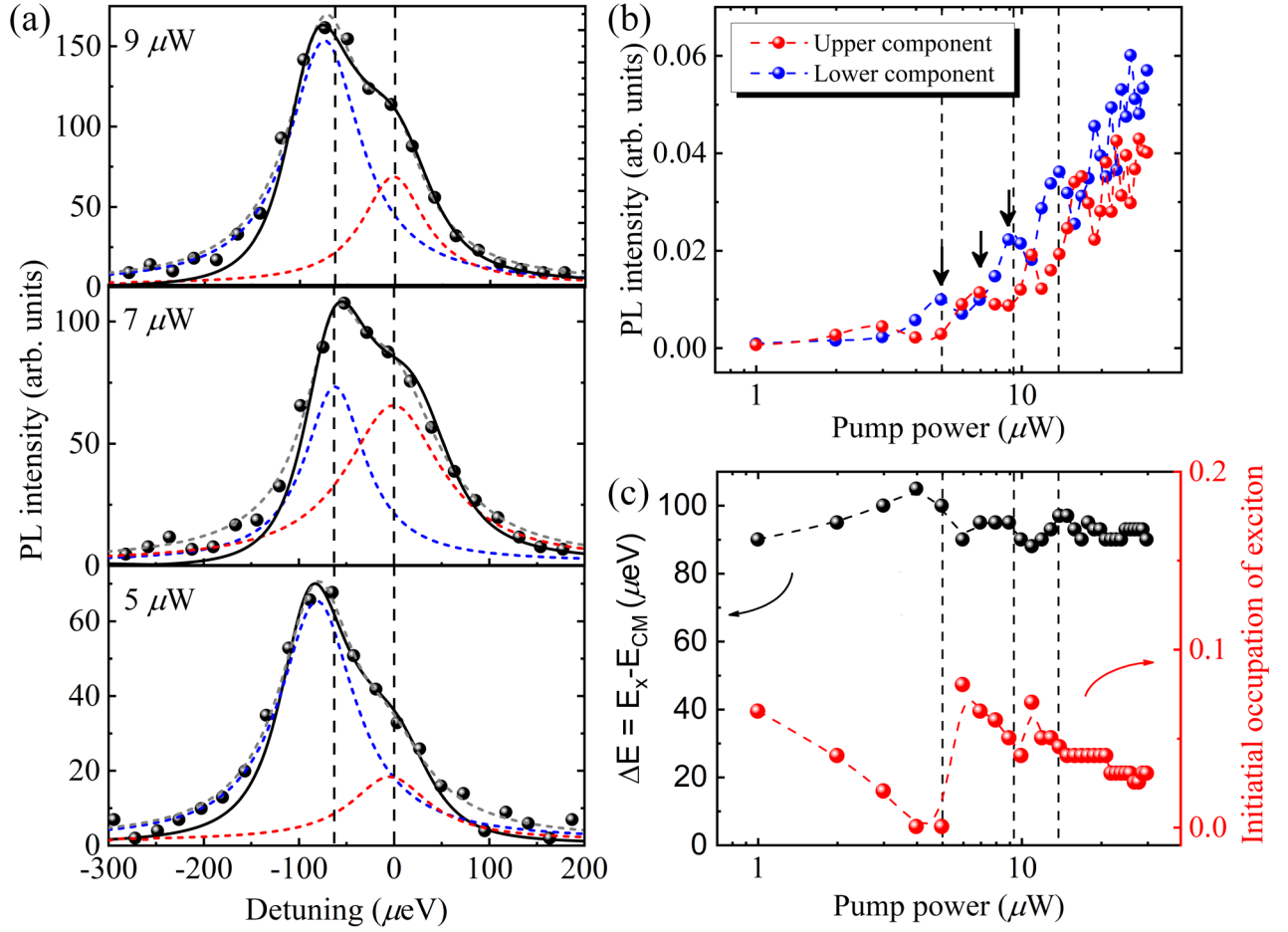


Figure 4 Power-dependent Rabi-like oscillation of the coupled QD-cavity (a) PL spectra (dot) of the nearly resonantly coupled QD and CM excited by the 900nm pulsed laser at average power 5 μW , 7 μW , and 9 μW . The blue and red dash curves are the double Lorentzian fitting with the accumulative fitting as the grey dash curve. The vertical dash line marks the energy of two branches at 7 μW . The black solid curve is from the cQED modeling. (b) Absolute PL intensity of upper and lower energy components branch as a function of average pump power extracted from (a), which reveals clear oscillation under low injection. The three arrows mark the pump power at 5 μW , 7 μW , and 9 μW . (c) Energy splitting between upper and lower components (black) and initial occupation of exciton in the coupled QD-cavity system (red) as a function of pump power extracted from the fitting by cQED modeling. The black and red dash curves are the guides to the eye. The vertical dash lines mark approximately the oscillation period.